Centimeter and Millimeter-Wave Propagation Characteristics for Indoor Corridors: Results From Measurements and Models

FEYISA DEBO DIBA[1,2], **MD ABDUS SAMAD**[1,3], **(Member, IEEE),**
AND DONG-YOU CHOI[1], **(Senior Member, IEEE)**

[1]Department of Information and Communication Engineering, Chosun University, Gwangju 61452, South Korea
[2]Department of Electronics and Communication Engineering, Adama Science and Technology University, Adama 1888, Ethiopia
[3]Department of Electronics and Telecommunication Engineering, International Islamic University Chittagong, Chattogram 4318, Bangladesh

Corresponding author: Dong-You Choi (dychoi@chosun.ac.kr)

ABSTRACT The millimeter-wave (mm-wave) frequency band is projected to play a critical role in next-generation wireless networks owing to its large available bandwidth. Despite the theoretical potential for high data throughput, the mm-wave frequency faces numerous challenges—including severe path loss and high penetration loss. Therefore, a reliable understanding of channel propagation characteristics is required for the development of accurate and simple indoor communication systems. In this study, we conducted measurement campaigns with unique transmitter- receiver combinations using horn and tracking antennas, at 3.7 and 28 GHz in an indoor corridor environment on the 10th floor of an IT building and the 3rd floor of the main building of Chosun University, Gwangju, South Korea, and the details are presented herein. In both line-of-sight and non-line-of-sight scenarios, the large-scale path losses, and small-scale channel statistics, such as root mean square delay spread, and number of clusters, were obtained using the measurement results in a waveguide structure indoor corridor environment. We have proposed alternate methodologies beyond classical channel modeling to improve path loss models using artificial neural network (ANN) techniques—to alleviate channel complexity and avoid the time-consuming measurement process. The presented regression successfully assists the prediction of the path loss model in a new operating environment using measurement data from a specific scenario. The validated results suggest that the ANN large-scale path loss model used in this study outperforms the close-in reference distance and floating-intercept (alpha-beta) models. Additionally, our result shows that the number of time clusters follows an Erlang distribution.

INDEX TERMS Path loss models, delay spread, time cluster, mm-wave propagation, artificial intelligence, indoor corridor.

I. INTRODUCTION

Wireless data stream is rapidly increasing worldwide—and by 2022, mobile data traffic is projected to reach 77.5 exabytes/month [1]. Most data traffic growth stems from evolving indoor wireless uses, such as wireless cognition, centimeter-level position location, and ultra-high-definition streaming. These wireless data traffic demand huge bandwidths that are enabled by millimeter-wave (mm-wave) bands in 5G and beyond [2], [3].

In outdoor to indoor communications, the signals propagate through walls, which causes considerable penetration

The associate editor coordinating the review of this manuscript and approving it for publication was Thomas Canhao Xu.

losses (of up to 60 dB) in mm-wave bands [4]. Therefore, it is advantageous to install separated indoor mm-wave communication networks from co-channel outdoor cellular links.

Millimeter-wave bands have been extensively studied [5]–[7] at 60 GHz—and applied in the IEEE 802.11ad/ay standards for wireless local area networks (WLANs) [8]. Few studies have also reported indoor channel modeling and measurements at other evolving mm-wave frequencies [9]. Precise channel models are important for the design and roll-out of 5G and other larger mm-wave bands.

Several path loss (PL) models are available in the literature, which are primarily categorized into three classes: deterministic, empirical, and semi-empirical PL models. Deterministic models are derived from the principles of physics, such as

Maxwell equations [10], uniform theory of diffraction [11], and ray tracing [12], and are computationally expensive and complex to implement. Empirical and semi-empirical models, such as the standard propagation model (SPM) [13], Okumura-Hata [14], WINNER II [15], ITU-R P.1812 [16], Stanford University Interim [17], Longley–Rice [18], and ITU-R P.1546 [19], that are predicted from a statistical analysis are computationally efficient and easy to implement. However, they may be less precise in some frequency bands and propagation environments. Furthermore, these models were created on a constrained timeline and did not reflect all of the important features of mm-wave channels. Further research and model refinements are required. Recently, artificial neural networks (ANNs) have been proposed to represent path loss more flexibly and accurately in different and complex propagation environments, such as indoor [20], rural [21], urban [22], and suburban [23].

The indoor environment differs from the outdoor environment in various ways. Indoor channel models must consider multipaths produced by scattering, refraction, reflection, shadowing, and penetration phenomena. This is as a consequence of the construction materials used, variations in floor plans, scale of smart devices used in the vicinity, people working and their movements, etc. [24]. Path loss prediction can be regarded as a regression problem, in which the parameters of the transmitter, receiver, frequency, buildings, etc., characterize the inputs, while the path loss represents the target output to be predicted. In the case of some parameters such as diffraction loss (DL), clutter loss is not well defined, and an ANN (black box) model based on learning is a useful tool for solving this type of regression problem and can be efficiently applied to indoor PL models [13].

The existing indoor path loss measurements were mostly based on very close transmitter to receiver ranges of less than 10 m steps [25], [26]. Additionally, most of the previous channel measurements used omnidirectional and directional antennas. However, owing to the sensitivity of mm-waves to dynamic blockage environments, a tracking antenna with steerable beam forming is required for proper system design and implementation [27].

Therefore, to obtain a general model in the mm-wave frequency regions, extensive characterization and modeling is necessary. The goal of this research is to examine channel characterization and path loss modeling in frequency ranges lower and higher than 6 GHz. We focused on characterizing the 3.7 and 28 GHz channel, because 3.5 GHz was assigned for 5 G roll out in South Korea—and 28 GHz was assigned for 5G use in the United States by the Federal Communications Commission (FCC). We used 3.7 GHz to avoid interference with the deployed 3.5 frequency.

Thus, this study has the following contributions:

- This article presents large-scale and small-scale propagation channel characteristics based on models and measurement campaigns with directional horn and tracking antennas at 3.7 and 28 GHz for two corridors scenarios.

- We proposed a new artificial neural network-based path-loss prediction model in indoor long corridors scenarios. The proposed model was compared with two well-known path loss models—the floating intercept (FI) and the close-in free space reference distance (CI). With respect to measurements, the signal fluctuation's standard deviation of the proposed ANN model around the average path loss was less compared to the existing path loss models, making it more accurate in predicting path loss.

- Small-scale channel statistics such as the number of time clusters and root mean square (RMS) delay spread were calculated from measured power delay profiles in both non-line-of-sight (NLOS) and line-of-sight (LOS) situations. The resulting channel statistics reveal that the number of time clusters follows an Erlang distribution.

The remainder of this article is organized as follows. Section II presents the indoor corridor measurement setup and procedures. Section III presents the path-loss models used in this study. Section IV presents the results and discussion of the work, and finally, Section V concludes the study.

II. MEASUREMENT EQUIPMENT, ENVIRONMENT, AND PROCEDURE DESCRIPTIONS

This section presents detailed parameters of the horn and tracking antennas, measurement campaigns, and measurement scenarios considered.

A. MEASUREMENT CAMPAIGN

We used three types of antennas for these measurements: a double-ridged waveguide directional horn antenna for a 3.7 GHz center frequency, a standard gain directional horn antenna, and tracking antennas for a 28 GHz operating frequency. We used a Keysight M5183B signal generator at the transmitter (Tx) side and Keysight PXI 9393A vector signal analyzer at the receiver (Rx) side in this measurement campaign, as depicted in Fig. 1

Measurements were performed three times. The first was at 3.7 GHz, using a horn antenna with a frequency range of 2 to 18 GHz at both the Tx and Rx sides. The second measurement was at a 28 GHz carrier frequency using a standard gain horn antenna with frequency ranging from 26 to 40 GHz at both the Tx and Rx sides. The third campaign used tracking consisting of 16-antennas at the Rx side and a standard horn antenna at the Tx side. The tracking antenna is used to collect a large amount of data per second to ensure the validity of the measured fast Fourier transform (FFT) spectral data. To collect the fastest FFT spectral data, Keysight Technologies used the PXIe high-performance vector signal analyzer (model name M9393A), applied a PC embedded in PXIe for faster data processing, and loaded the equipment operating program into the embedded PC. For 16 antenna (1ch) configurations, we collected and stored more than 600 full-bearing FFT (512 point) spectral data per second (at 2 MHz Span or higher) on the PC. The stored data are recorded along with

TABLE 1. Horn and Tracking antennas specifications and parameters descriptions.

Parameters	3.7 GHz	28 GHz	28 GHz (TAS)
Antenna type	horn	horn	tracking
Antenna model	BWAO218-10	WR 28-20A	tracking
Bandwidth (MHz)	1	1	2
Freq. band (GHz)	2–18	26.5–40	26.5–40
Tx/Rx Gain (dBi)	10	20	20
Transmit power (dBm)	7.2	10.6	10.6
Tx height (m)	1.75	1.75	1.75
Rx height (m)	1.5	1.5	1.5
Beam width (3 dB)	V 45°	V 20°	‡16-22.5°
Beam width (3) dB	H 40°	H 18°	◁16-22.5°
Tx cable loss(dB)	2.8	9.4	9.4
Rx cable loss(dB)	2	6.2	6.2
Polarization	H-H†	H-H†	H-H†

†Co-polarization, ‡E-plane, ◁H-plane.

each antenna-specific data collected during the move—-as well as orientation and location information so that the map can display the direction of the transmission point according to the maximum reception level. In addition, the measured data can be used to oust the best signal for each antenna for a specific time, allowing the moving average, vehicle binning conversion, and display of the coverage markings on the map at intervals. Fig. 2 illustrates the connection between the Tx and Rx through tracking and standard horn antennas. From Fig. 2 the signal generator (SG) connected to horn antenna which transmits the signal to tracking antenna systems (TAS) through wireless. TAS, which is the receiver, forward the signal to signal analyzer (SA) via hub and finally displayed on the monitor. Table 1 lists the equipment specifications and parameter configurations.

B. EXPERIMENTAL SCENARIO AND PROCEDURES

The measurement scenarios were formulated based on the requirement to construct large-scale and small-scale channel models that consider path loss and multipath propagation properties in wave guide-like structures for future networks. As a result, we selected an internal corridors with metal doors, dry concrete walls and ceilings, and tiled floor. In the corridors, a propagating signal flows from Tx to Rx via the LOS (direct) and NLOS (reflected, dispersed, and/or diffracted) routes. A propagating signal in a closed plan

environment must pass via an obstruction to reach the receiver resulting in shadowing [9]. Therefore, this study is focused on the propagation characteristics, specifically an interior corridors with modal attenuation, using measurements and models. First, LOS propagation parameters were calculated for scenarios in which there was no obstacle between Tx and Rx, and they were pointed in the same direction with bore sight alignment. The NLOS propagation parameters were then determined when the Tx and Rx antennas were out of alignment on boresight. Finally, the strongest signal strength measured from tracking antennas for each exclusive antenna pointing angle in every Tx and Rx combination was used to calculate the best path loss [9].

In this study, we conducted measurement campaigns on the 10th floor of the IT and convergence engineering building, as shown in Fig. 3, and on the 3rd floor of the main building—Chosun University, South Korea. The main building is 375 m long which is the most extended building in Guinness book of records. We took measured data up to 260 m at 10 m and 20m intervals of the following 18 measurement points. 14, 20,30,40,50,60,70,80,90,100,120,140,160,180,200,220,240, and 260 m. The IT building is 100 m long and we took measurements up to 90 m such as 14, 20,30,40,50,60,70,80,90 in 10-meter increments per measuring location for 9 LOS measurement points. To measure the NLOS, we have placed the mobile TAS receiver and the horn antenna inside 4 rooms of IT building namely: 1021, 10225, 10228_1, and 10228. The minimum distance from the transmitter to receiver was 59.48, 84. 94,88.25, and 94.54 m for the rooms 10221, 10225, 10228_1, and 10228, respectively.

The measurement environments were typical wave guide-like structured indoor corridors with floors, walls, metal office doors, a stairwell, and an elevator (see Fig. 3). The width, length, and height of the indoor corridor of the IT building were 2.54, 100, and 2.7 m, whereas those of the main building were 2.9, 375, and 3.43 m, respectively. The Tx and Rx antennas were installed at 1.75m and 1.5 m above the floor by fixing the Tx antenna at one end of the corridor, and locating the Rx antenna at various places for both NLOS and LOS measurements. The measurements were conducted at the same Tx and Rx sites for both the 3.7 and 28 GHz frequencies to make direct comparisons between the two frequency bands. Horizontal polarization was used at both the Tx and Rx antennas in the measurement tests. We placed Tx in a single location and Rx in 9 different locations for LOS and 4 for NLOS for conducting the IT building measurements. For the main building measurements, Rx was located at 18 different places in the LOS measurements.

The received power measurement data were post-processed at every location along the corridor's axial length in 10 m steps from Tx to Rx. To ensure high-quality data gathering, the measurement device was rigorously calibrated, and the measurements were repeated and averaged. The average received power from the dataset at each measurement point was calculated. Finally, by converting the power received,
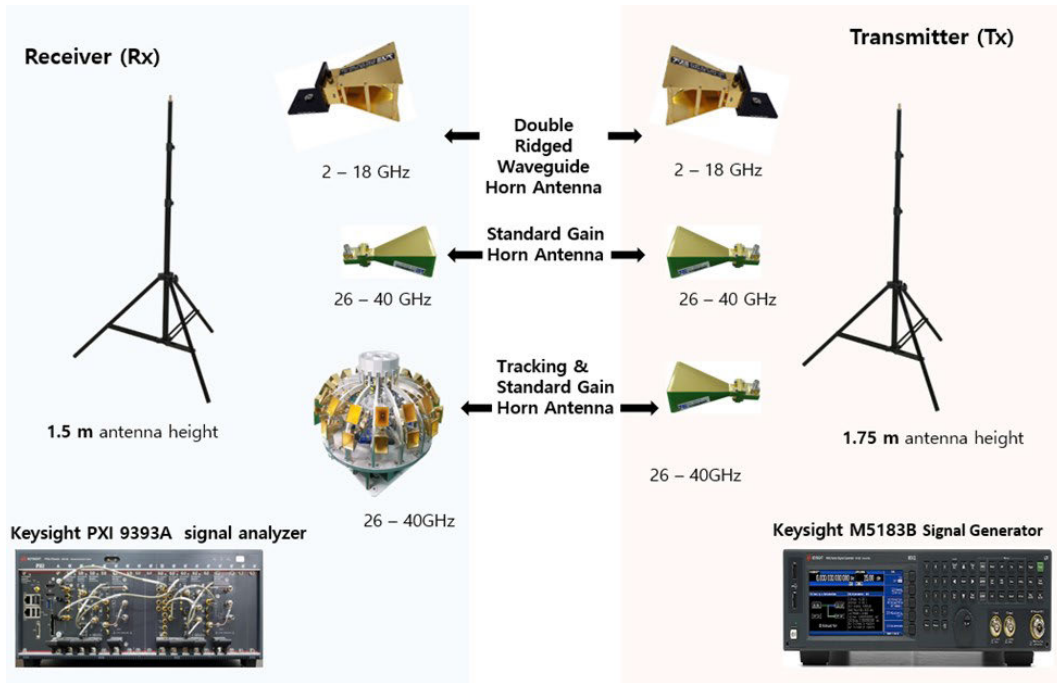
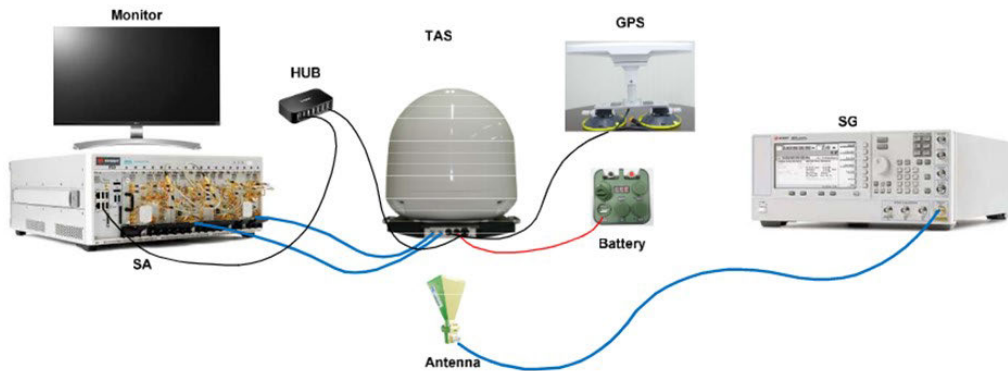**FIGURE 1.** Horn and tracking antennas used in the measurements.

FIGURE 2. Tracking antenna set up for measurements.

the path loss was computed at each site. LOS and NLOS environments were used in the tests.

III. CHANNEL MODELS

This section presents the temporal channel characteristics and path loss of the 3.7 and 28 GHz bands in the two experimental sites. They were analyzed in terms of channel parameters, such as path loss, the number of clusters, and multipath component (MPC) delay spread, based on the received signal power measurements using the horn and tracking antennas.

A. LARGE SCALE PATH LOSS MODELS

In radio channel models for evaluating the link budget and coverage in a cellular network, path loss is a critical component. The path loss for each site was calculated using the measured data, as follows:

$$PL = P_{(Tx)} - P_{(Rx)} + G_{(Tx)} + G_{(Rx)} - L_{(c)} \qquad (1)$$

where P_{Tx} is the transmitted signal power, and P_{Rx} is the received signal power calculated by integrating the energy of the paths. G_{Tx} and G_{Rx} are the gains of the antennas used during the transmitting and receiving processes, respectively. Additionally, L_c is transmitter and receiver cable losses. By integrating the powers of all the synthesized pathways, we can successfully determine the directional path loss [28]. To properly design wireless communication systems, path loss models are required to calculate the attenuation of propagating signals with distance. It is desirable to gain as wide a measurement range as feasible for new wireless networks to ensure model correctness across long distances. The FI

(alpha-beta) model and CI free space reference distance model are two common empirical path loss models to fit measured PLs [29].

1) CI PATH LOSS MODEL

The CI free-space reference is a common and superior large-scale path loss model over various frequency bands and environments [30]. In this work, we use the CI path loss model with a 1 m distance reference, as expressed in (2).

$$PL^{CI}(d) = 32.4 + 20 \log_{10}(f) + 10n \log_{10}(d) + X_\sigma^{CI} \quad (2)$$

where X_σ represents the shadow fading in dB, modeled with Gaussian random variable at zero mean and σ represents the standard deviation, n denotes path loss exponent (*PLE*), at carrier frequency f in GHz and, at distance d in meter.

2) FI PATH LOSS MODEL

Researchers who worked on the development of the 3GPP and WINNER II channel models [31] employed the *FI* model. The *FI* model uses a least-squares regression method to determine the best fit line to the experimental data, extracting two parameters, slope and an intercept,

to derive the equation [29], [32]:

$$PL^{FI}(d) = \alpha + 10\beta(d) + X_\sigma^{FI} \quad (3)$$

where β is the line slope (different from the PLE), α is the float-intercept in dB (different from the FSPL reference), and X_σ^{FI} is a zero mean Gaussian random variable with shadow fading that signal changes over time in relation to the typical large-scale path loss. Previous studies have shown that the *FI* and *CI* path loss models provide almost similar standard deviations for shadow fading in outdoor mm-wave channels [29], [32]–[34]. The *CI* and *FI* parameters such as n, α, β and σ are derived using minimum mean square error (MMSE) which fits the data from measurements with small errors.

3) PROPOSED ANN PATH LOSS PREDICTION MODEL

Path loss prediction modeling can be assumed as a regression problem for mapping the relationship between the values of path loss and input link parameters, such as path length, operating frequency, attenuation, reflection [35], [36]. In the literature, there are two primary regression techniques. The first is multivariate linear regression, which determines a mathematical formula that explicitly defines path loss as a linear function of input parameters. The second method relates the input and output by a black box without any explicit mathematical formulation [37]. This is an interesting method that mimics the system behavior without any descriptive value and is suitable in the case of a poorly defined or poorly identified phenomenon.

In this study, we propose a second technique for path loss prediction. This is because parameters, such as diffraction loss (DL) and its dependence on the geometric form of the knife edge, along with clutter loss and its dependence on frequency, are not well defined. Therefore, the learning-based black box model can be efficiently used to predict the wave propagation path loss, and is a convenient tool for solving this type of regression problem. Fig. 4 shows a simple neural network that is mathematically expressed as follows:

$$Y = w^T X + e \quad (4)$$

where Y denotes the dependent response, and $X = (x_1, x_2 \ldots, x_n)$ is the input to the network which includes channel state information (CSI) features such as, received power, link distance, time delay, RMS delay spread, and frequency. The input X is multiplied by transposed (T) weights vectors $W = (w_1, w_2 \ldots, w_n)$ plus a neuron bias e to produce Y. The output path loss is predicted by mapping Y to the activation function. We consider the following sigmoid function to predict path loss.

$$PL^{ANN} = \frac{1}{1 + e^{-Y}} \quad (5)$$

where Y and PL^{ANN} represent the transformation and activation (path loss) functions of the layer, respectively.

The error between the measured PL^M and the predicted PL^{ANN} path losses is determined using the loss function
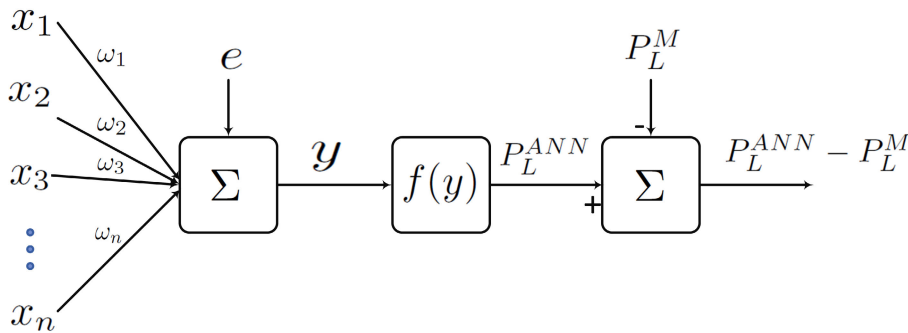
FIGURE 4. Simple artificial neural network.

$L(PL^{ANN}, PL^M)$. The squared error can be utilized as a loss function in regression analysis problems, as seen below [38]:

$$L(PL^{ANN}, PL^M)) = \frac{1}{2N}\left[\sum_{i=1}^{n}(PL_i^{ANN} - PL_i^M)^2\right] \quad (6)$$

The slope and variance of the path loss model can be determined using linear regression, where distance is the only channel feature used to estimate the model. Then, the slope and variance can be predicted [39].

$$\beta = (X^T X)^{-1} X^T PL \quad (7)$$

where, X^T is transposed input parameters. We may deduce the standard deviation σ from the given estimate to obtain the shadow fading parameter.

$$\sigma = \sqrt{\frac{1}{N}\left[\sum_{i=1}^{n}(PL - \mu)^T(PL - \mu)\right]} \quad (8)$$

After obtaining these parameters, we were able to compare an ANN path loss model to *CI* and *FI* path loss models.

B. TEMPORAL STATISTICAL CHANNEL MODELS
In this section, the RMS delay spread and the number of time clusters were determined from the measured data at an operating frequency of 28 GHz.

1) RMS DELAY SPREADS
The RMS delay spread is used to characterize the time dispersion properties of wideband channels because it is a suitable indicator of coherence bandwidth nature and time dispersion and of the multipath channels, as well as a measure of how serious inter-symbol interference could be—-according to the signal bandwidth [40]. A recent study reported that determining the specific beam-pointing directions that provide both minimum multipath delay spread and minimum path loss could be advantageous in building power-efficient mm-wave mobile communication systems with simple equalization [41]. The channel RMS delay spread and other time dispersion parameters generally determine the physical layer design; further, analyzing these qualities can offer useful information for the design of indoor mm-wave networks.

In this section, RMS delay spreads and temporal statistics are considered for conventional LOS and NLOS settings.

The RMS delay spread is derived from the second moment of the power delay profile as follows [40]:

$$\tau_m = \frac{\sum_i P(\tau_i)\tau_i}{\sum_i P(\tau_i)} \quad (9)$$

$$\tau_c = \frac{\sum_i P(\tau_i)\tau_i^2}{\sum_i P(\tau_i)} \quad (10)$$

$$\tau_{rms} = \sqrt{\tau_c - \tau_m^2} \quad (11)$$

where $P(\tau_i)$ is the received signal power (in mW) with respect to the time delay τ_i, τ_m is the mean excess delay, and τ_c is the second central moment of a PDP.

2) NUMBER OF TIME CLUSTERS
A cluster is described as a group of multipath components (MPCs) closely spaced in the joint temporal-spatial domain, with each cluster originating from a reflector or scatterer in the environment—-according to current standard documents, such as the 3GPP TR 38.901 channel model [7], [42]. A temporal cluster (TC) comprises MPCs that arrive simultaneously from different time slots [43].

In the time domain, the partition is accomplished by defining a minimum inter-cluster time void interval (MTI). If the excess time delays of two consecutively recorded MPCs differ by more than MTI, they belong to two different TCs. These two MPCs are the last of the former TC's MPCs and the first of the latter TC's MPCs. In an outdoor urban microcell (UMi) case, for instance, 25 ns was applied as MTI [43]. Meanwhile, 6 ns was taken as MTI for an indoor conditions [28].

IV. RESULTS AND DISCUSSION
Radio wave propagation channel modeling parameters are vital tools for planning more efficient next generation wireless communication systems. They can predict signal attenuation while propagating over a link distance. In the corridor scenario, the geometry and conductivity of the construction materials guide the wave propagation from the Tx to the Rx. The indoor corridor propagation environments cause

multipath due to diffraction, reflections, shadowing effects, and penetration loss, all of which have substantial effects on the received signal power [44]. Owing to the wave guide impacts and multipath reflection, the received signal is regarded as the sum of the reflected and direct waves from the Tx. Several existing path loss channel models are based on free space, scattering, and reflection in a ray tracing method over short distances of a few meters [45], [46]. In this study, we derive channel statistics based on extensive radio wave measurements for indoor corridor environments at 3.7 and 28 GHz frequency bands, and we propose an ANN model for path loss prediction. To study the received power loss over a link distance at each operating frequency, the FI and CI free-space reference distance path loss models and the proposed ANN model were used. The performances of these models were compared with the measured path loss for each horn and tracking antennas.

A. PATH LOSS MEASUREMENTS AND MODELS

1) PATH LOSS MEASUREMENTS AND MODELING FROM HORN ANTENNAS

A horn antenna comprises a bell-shaped metal waveguide, such as a horn, to guide radio wave propagation in a beam. Horn antennas are primarily used as antennas at microwave frequencies and a UHF of above 300 MHz. They provide a high gain, ranging from 10 to 20 dB, and up to 25 dB in some cases, with a directional radiation pattern.

In this study, we implemented a double-ridged waveguide horn antenna and a standard gain horn antenna with frequency bands of 2-18 GHz and 26-40 GHz, respectively. The measurement campaigns were conducted at 3.7 and 28 GHz to study wave propagation in indoor corridors and to launch more accurate path loss models. Wave propagation analysis was performed for the LOS and NLOS paths.

First, we analyzed the measurement data of 9 and 18 Rx LOS sites for the IT and main building corridors, respectively—-with 32 azimuth orientations per Rx place for a fixed Tx location at each of the operating frequency. Table 2 presents the regression parameters of the three models for different scenarios.

For the CI free space reference path loss model, the IT building horn antenna measurements provide PLEs of 1.53 and 2.976 for the LOS and NLOS paths, respectively, at the 3.7 GHz frequency band. At 28 GHz, the PLEs are 1.78 and 3.896 for the LOS and NLOS paths, respectively. For the LOS paths, the PLEs are less than 2 (the theoretical free space value) for both the 3.7 and 28 GHz frequency bands. This indicates that radio wave propagation in indoor corridor environments provide constructive interference from ceiling and floor bounce reflections. For NLOS, the PLEs are 2.96 and 3.896 for the 3.7 and 28 GHz frequency bands, respectively, which are considerably higher than those of LOS PLEs. The higher PLE values at 28 GHz indicate greater reflection and penetration losses from the wall, ceiling, and floor. The shadowing standard deviation values at 3.7 GHz are

8.65 and 3.071 for LOS and NLOS, respectively. At 28 GHz the shadowing deviations values are 4.754 and 15.93 for LOS and NLOS, respectively. This indicates that the 28 GHz NLOS CI model provides a substantially larger shadow fading standard deviation, which is approximately 16 dB, demonstrating much higher received signal strength fluctuations around the mean received power over all T-R separations. These results show that a greater path loss for 28 GHz than that for the 3.7 GHz signal, and the NLOS shows more path loss than the LOS. This is because the higher frequency signals have shorter wavelengths. Thus, their energy is lost due to collisions in the medium in which it travels.

Table 2 also lists the FI model parameters. It is observed that α values differ from the free space path loss at 1 m in LOS at 3.7 GHz (79.5 dB compared to the 43.76 dB theoretical FSPL at 1 m) and at 28 GHz (70.2 dB compared to the 61.4 dB theoretical FSPL at 1 m). This highlights the FI model's lack of insight when it comes to reconciling the physical impacts of polarization and environmental degradation with distance. Furthermore, in NLOS environments, the slope values (β) is less than the free space ($\beta = 2$) for both 3.7 and 28 GHz. This does not adequately predict the intuitive reality that NLOS links suffer from significant loss with distance than free space signals. A paucity of measurements or data samples often leads to inaccurate measurements [29], [32]. The parameters of the very sensitive FI model can also be dramatically changed by post-processing procedures that use different thresholding strategies [29].

In addition, Table 2 presents the slope and standard deviation values of the ANN model for the IT and main building in both the LOS and NLOS conditions. In comparison to the CI reference and FI models, the signal fluctuation's standard deviation of the proposed ANN model around the average path loss was less, making it more accurate in predicting path losses. The ANN model improved the standard deviations for 3.7 GHz NLOS by 724% and 10.64% compared to CI and FI models, respectively. At 28 LOS IT building, it improved by 4.68% and 9.76% compared to CI and FI models, respectively. Further, the β values of the ANN are closer to the free space theoretical value than the β values of the FI model. Figs. 5,6,7,8 illustrate the scatter plots of the LOS path loss from models and measurement campaigns for the IT and main building indoor corridor scenarios. The Figures show the path loss results comparisons among the measured CI and FI, and proposed ANN models for the IT and main building environments.

Fig. 9 shows the NLOS path loss plot at 3.7 GHz for the IT building, which shows that the NLOS has more of a path loss than LOS at the same frequency and building, as shown in Fig. 5. It is observed that when the proposed ANN model is compared with, and evaluated against the existing models—-such as CI and FI—-it demonstrates good performance and agrees well with the measured path losses for both the LOS and NLOS conditions. As seen from the figures, the path loss rises at the beginning owing to less wave guiding effects of the reflected and diffracted waves
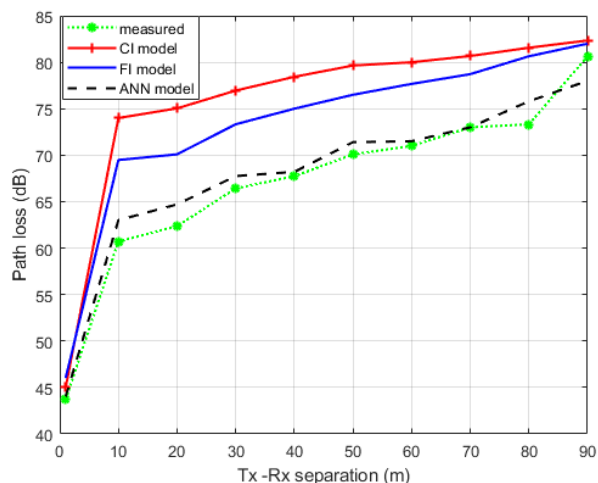
FIGURE 5. 3.7 GHz LOS large scale path loss for IT building corridor with horn antenna.
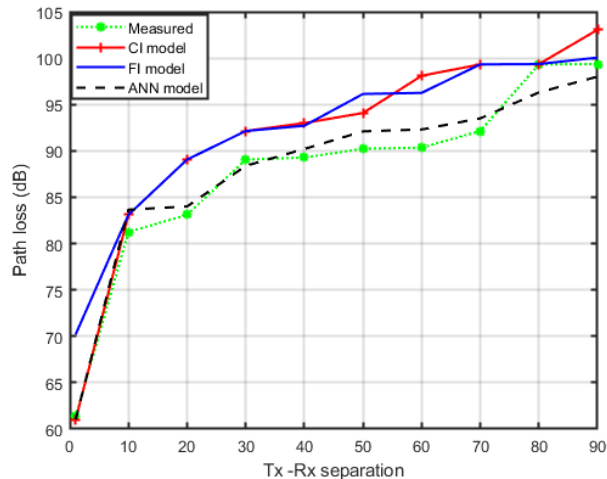

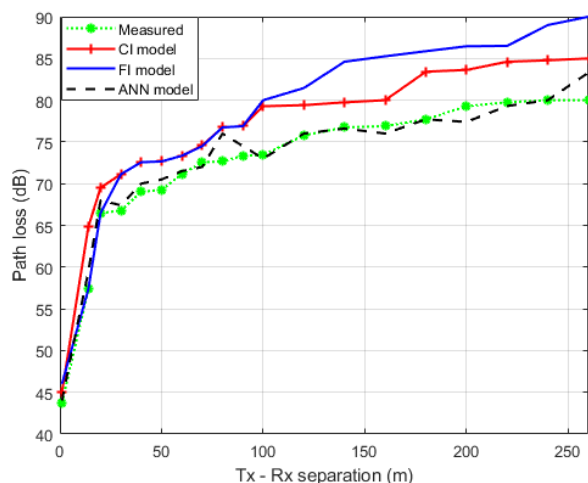**FIGURE 7.** 28 GHz LOS large scale path loss for IT building corridor with horn antenna.

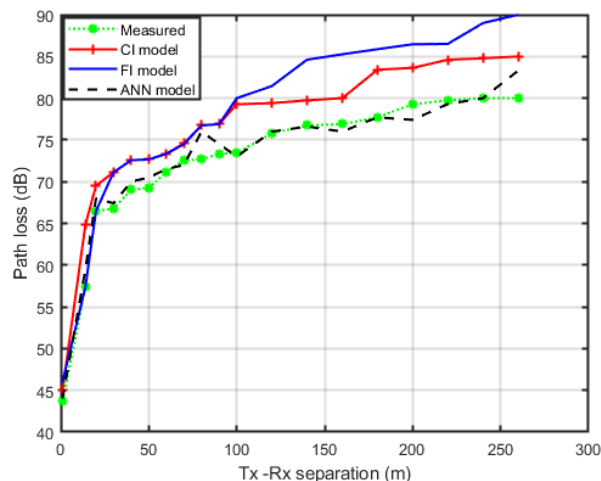**FIGURE 6.** 3.7 GHz LOS large scale path loss for main building corridor with horn antenna.

FIGURE 8. 28 GHz LOS large scale path loss for main building corridor with horn antenna.

by the corridor. However, as the link separations increase, the guided wave maintains the signal strength across the corridor—-resulting in a lower increase in path loss. Initially, for both the 3.7 GHz and 28 GHz bands, multipaths had no significant effect on path loss because high-order modes were considerably suppressed over short link lengths as shown in Figs. 5,6,7,8.

Comparing the two buildings (IT and main), the main building shows better performance than the IT building at both the 3.7 and 28 GHz frequencies. For instance, at 3.7 GHz, the maximum path loss for the IT building is approximately 80 dB; whereas that for the main building is approximately 100 dB. This is due to the corridor building dimensions, stronger constructive interferences, and that better wave-guiding effects were experienced in the corridor with higher dimensions. In general, the signal attenuates more at a high band of 28 GHz than at a low band of 3.7 GHz, and NLOS shows more path loss than LOS, as expected.

2) PATH LOSS MEASUREMENTS AND MODELING USING TRACKING ANTENNAS

When wireless channel measurement is performed with a mm-wave omnidirectional antenna, it is difficult to obtain sufficient gain—-therefore, a horn antenna with a specific beam width must be applied. TA Engineering, Inc. has adopted two types of horn antennas with beam widths of 18° to 22.5° or 45°. In most mm-wave field measurement systems, the directional steerable horn antenna is attached to a rotator, but this does not provide sufficient valid data to ensure accurate measurements. TA Engineering has arranged the horn antenna in a circular shape with 8 × 1, 8 × 2, 16 × 1, and 16 × 2 antennas—-and a high-speed MW switch (20 ns) was used to automatically select antennas and collect the fast Fourier transformation (FFT)-based spectrum data from the incoming signal. Therefore, in this study, we adopt tracking antennas with 8 × 2 arrangements for the 28 GHz center frequency.

TABLE 2. Horn antennas regression parameters of the three path loss models over corridors at 3.7 and 28 GHz.

Frequency	Paths	CI-model		FI-model			ANN-model	
		n	σ	α	β	σ	β	σ
3.7 GHz	LOS-IT	1.53157	8.65	79.53	0.608	7.8	2.25	6.08
3.7 GHz	LOS-M	1.512	7.75	21.94	2.601	8.24	1.2	6.16
3.7 GHz	NLOS-IT	2.976	6.071	100.307	0.00363	6.5	1.25	5.25
28 GHz	LOS-IT	1.7817	6.754	70.2	1.2517	7.481	2.75	6.15
28 GHz	LOS-M	2.033	9.37	27.4	3.727	28.71	1.65	7.61
28 GHz	NLOS-IT	3.896	15.93	119.2	0.845	25.45	1.75	13.2

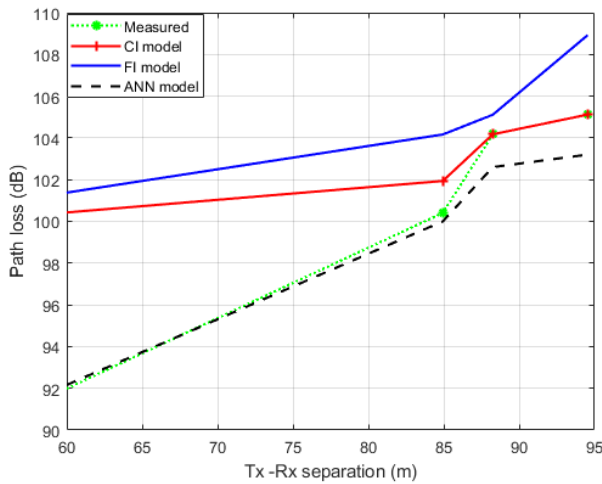**FIGURE 9.** 3.7 GHz NLOS large scale path loss for IT building corridor with horn antenna.

FIGURE 10. 28 GHz best large scale path loss for IT building corridor with tracking antenna.

Multiple copies of the transmitted signal arrive at the Rx by diverse pathways in a typical RF environment, resulting in multipath components (MPCs). When compared to omni-directional antenna, the Rx of directional tracking antenna catches less MPCs due to its directionality. This minimizes the delay spread, which is defined as the time difference between the earliest and latest important MPCs arriving. The narrower the beam, on the other hand, the more probable there will be beam misalignment between the Rx and the Tx. As a result, the number of captured MPCs at the Rx decreases, affecting the delay spread.

Table 3 provides the CI, FI and ANN path loss models for 16 receiver tracking antennas, where A stand for antenna at 28 GHz measurement campaigns. Antenna 1 (A_1) and best antenna position give PLEs of 1.76 and 1.698, respectively. This shows that the first and best antenna positions provide constructive interference from the ceiling and floor bounce reflections. For the rest of the antenna positions, the PLES were greater than 2. This is due to the difficulty of correctly aligning very thin beam tracking antennas to the boresight at the T-R separation distances observed, indicating the sensitivity of beam pointing in future mm-wave wireless systems.
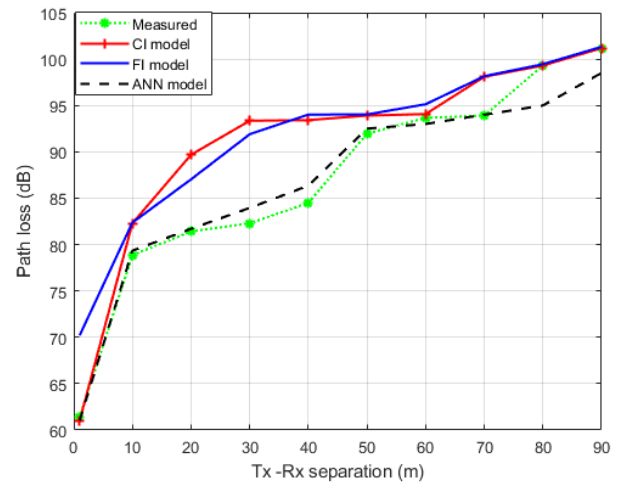
Again, in comparison to the CI reference and float intercept models, the signal fluctuation's standard deviation of the proposed ANN model around the average path loss was less by 4.28 % than that of the CI reference and FI models.

Fig. 10 shows the path loss using the tracking antenna, which clearly shows that the path loss from this Figure is less than that of Figs. 7 and 8 for the same operating frequency but different receiving antennas. This demonstrates that the tracking antenna exhibits less path loss compared to the path loss from the horn antenna owing to the effective beam pointing in the tracking antennas.

B. RMS DELAY SPREADS AND TC CLUSTER RESULTS
Fig. 11 illustrates the cumulative distribution functions (CDF) for the RMS delay spreads of the PDPs measured at 28 GHz for the IT building indoor corridor. It shows that, in both the LOS and NLOS scenarios, 90% of the measured RMS delay spreads are less than 30 ns. Because impediments in NLOS places prevented or significantly attenuated the direct channel, in allowing arrival of multipath at the receiver over a longer propagation time span, NLOS places were shown to have larger RMS delay spreads than LOS sites.

TABLE 3. Tracking antennas regression parameters of the three path loss models over corridors at 28 GHz.

| Antennas	CI-model		FI-model			ANN-model	
	n	σ	α	β	σ	β	σ
A1	1.76	4.64	55.58	2.1	4.52	2.685	3.68
A2	2.52	7.07	89.54	0.83	4.95	3.2	4.52
A3	2.77	8.37	99.12	0.51	4.92	3.36	4.12
A4	3.04	5.46	74.57	2.25	4.92	3.32	4.26
A5	2.9	7.27	90.7	1.14	6.86	3.34	6.05
A6	3.31	9.14	109.3	0.44	3.18	3.63	3.38
A7	3.35	7.5	97	1.22	3.96	3.57	3.35
A8	2.82	7.71	85.1	1.4	6.43	3.27	7.63
A9	2.12	7.15	94.92	0.11	3.87	3.05	3.88
A10	2.62	9.99	99.55	0.34	7.27	3.24	7.34
A11	3	8.6	104.5	0.412	3.75	3.46	3.94
A12	3	8.32	100.6	0.66	4.47	3.45	3.87
A13	2.93	9.07	102.5	0.465	5.28	3.4	4.46
A14	2.95	5.66	87.5	1.38	3.18	3.35	3.17
A15	3.06	7.85	85.16	1.64	6.59	3.35	6.16
A16	2.38	5.48	66.08	2.1	5.42	3.0	5.22
A-best	1.698	3.9	59.66	1.798	3.9	2.6	3.58
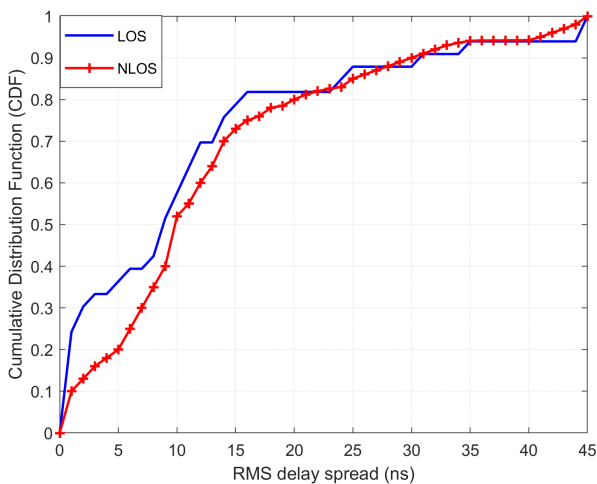
FIGURE 11. Cumulative distribution functions (CDF) against RMS delay spreads.
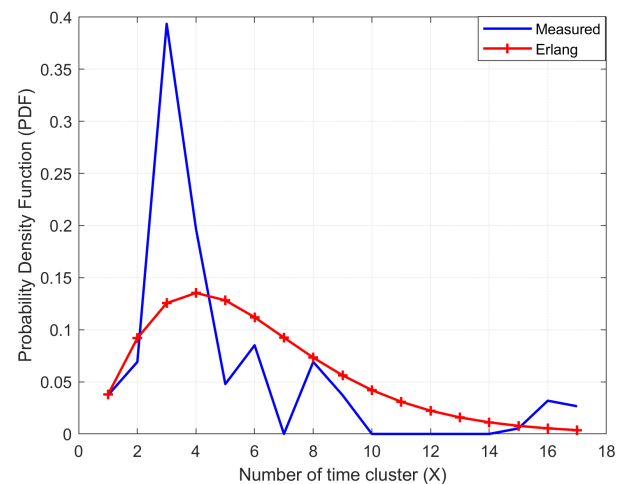

FIGURE 12. Probability distribution against number of time cluster.

The number of time clusters, or TCs, is determined by splitting the measured PDPs according to MTI. The erlang distribution is shown to be well fitted by the probability density distribution of the number of TCs (X) at 28 GHz for the LOS scenario with a 6 ns MTI in Fig.12. The Erlang distribution's probability density function is given as:

$$f(X, K, \lambda) = \frac{\lambda^k X^{K-1} e^{-X\lambda}}{(K-1)!} \quad (12)$$

where the parameter λ is called the rate parameter, and the parameter k is called the shape parameter.

V. CONCLUSION

This study is aimed at developing accurate channel models by investigating the channel propagation characteristics at 3.7 and 28 GHz bands for indoor corridors. Radio propagation measurements and analysis were performed to explore the characteristics of the indoor channels. Horn and tracking

antennas were used to perform the LOS and NLOS received signal power measurements. A supervised artificial neural network was proposed to predict path loss in indoor scenarios. Based on the experimental measurements, the CI, FI, and ANN path loss models were analyzed and compared. In comparison to the CI reference and FI models, the signal fluctuation's standard deviation of the proposed ANN model around the average path loss was less, making it more accurate in predicting path loss. For tracking antennas, antenna 1 and the best antenna position produced PLEs of 1.76 and 1.698, respectively. This shows that the first and best antenna positions provide constructive interference from the ceiling and floor bounce reflections. For the remaining antenna positions, the PLEs were greater than 2. This is due to the difficulty of accurately aligning very thin beam tracking antennas to their boresights at the T_x-R_x separation distances observed, indicating the sensitivity of beam pointing in future mm-wave wireless systems. In all measurement settings, path loss result comparisons among the measured CI, FI, and proposed ANN models resulted in the proposed model outperforming the CI and FI path loss models. We conducted a detailed analysis of the channel characteristics—-including path loss, RMS delay spread, and time cluster. In general, the signal attenuates more at a high band of 28 GHz than at a low band of 3.7 GHz, and NLOS shows more path loss than LOS, as expected. The tracking antenna exhibits less path loss than the horn antenna. The study of micro- and mm-wave propagation characteristics will aid in the comprehension of radio channels and the development of mm-wave communication systems.

REFERENCES

[1] G. Forecast, "Cisco visual networking index: Global mobile data traffic forecast update, 2017–2022," *Update*, vol. 2017, p. 2022, Feb. 2019. [Online]. Available: https://cyrekdigital.com/uploads/content/files/white-paper-c11-741490.pdf

[2] T. S. Rappaport, Y. Xing, O. Kanhere, S. Ju, A. Madanayake, S. Mandal, A. Alkhateeb, and G. C. Trichopoulos, "Wireless communications and applications above 100 GHz: Opportunities and challenges for 6G and beyond," *IEEE Access*, vol. 7, pp. 78729–78757, 2019, doi: 10.1109/ACCESS.2019.2921522.

[3] O. Kanhere and T. S. Rappaport, "Position location for futuristic cellular communications: 5G and beyond," *IEEE Commun. Mag.*, vol. 59, no. 1, pp. 70–75, Jan. 2021, doi: 10.1109/MCOM.001.2000150.

[4] K. Haneda, J. Zhang, L. Tan, G. Liu, Y. Zheng, H. Asplund, J. Li, Y. Wang, D. Steer, C. Li, and T. Balercia, "5G 3GPP-like channel models for outdoor urban microcellular and macrocellular environments," in *Proc. IEEE 83rd Veh. Technol. Conf. (VTC Spring)*, May 2016, pp. 1–7. [Online]. Available: https://arxiv.org/pdf/1602.07533.pdf

[5] H. Xu, V. Kukshya, and T. S. Rappaport, "Spatial and temporal characteristics of 60-GHz indoor channels," *IEEE J. Sel. Areas Commun.*, vol. 20, no. 3, pp. 620–630, Apr. 2002, doi: 10.1109/49.995521.

[6] S. Geng, J. Kivinen, X. Zhao, and P. Vainikainen, "Millimeter-wave propagation channel characterization for short-range wireless communications," *IEEE Trans. Veh. Technol.*, vol. 58, no. 1, pp. 3–13, Jan. 2009, doi: 10.1109/TVT.2008.924990.

[7] X. Wu, C.-X. Wang, J. Sun, J. Huang, R. Feng, Y. Yang, and X. Ge, "60-GHz millimeter-wave channel measurements and modeling for indoor office environments," *IEEE Trans. Antennas Propag.*, vol. 65, no. 4, pp. 1912–1924, Apr. 2017, doi: 10.1109/TAP.2017.2669721.

[8] A. Maltsev, A. Pudeyev, A. Lomayev, and I. Bolotin, "Channel modeling in the next generation mmWave Wi-Fi: IEEE 802.11 ay standard," in *Proc. 22th Eur. Wireless Conf.*, May 2016, pp. 1–8. [Online]. Available: https://mentor.ieee.org/802.11/dcn/16/11-16-1388-00-00ay-implementation-of-channel-models-for-ieee-802-11ay.doc

[9] G. R. Maccartney, T. S. Rappaport, S. Sun, and S. Deng, "Indoor office wideband millimeter-wave propagation measurements and channel models at 28 and 73 GHz for ultra-dense 5G wireless networks," *IEEE Access*, vol. 3, pp. 2388–2424, 2015, doi: 10.1109/ACCESS.2015.2486778.

[10] J. M. Gorce, K. Jaffres-Runser, and G. D. L. Roche, "Deterministic approach for fast simulations of indoor radio wave propagation," *IEEE Trans. Antennas Propag.*, vol. 55, no. 3, pp. 938–948, Mar. 2007, doi: 10.1109/TAP.2007.891811.

[11] W. M. O'Brien, E. M. Kenny, and P. J. Cullen, "An efficient implementation of a three-dimensional microcell propagation tool for indoor and outdoor urban environments," *IEEE Trans. Veh. Technol.*, vol. 49, no. 2, pp. 622–630, Mar. 2000, doi: 10.1109/25.832994.

[12] T. K. Sarkar, Z. Ji, K. Kim, A. Medouri, and M. Salazar-Palma, "A survey of various propagation models for mobile communication," *IEEE Antennas Propag. Mag.*, vol. 45, no. 3, pp. 51–82, Jun. 2003, doi: 10.1109/MAP.2003.1232163.

[13] M. Ayadi, A. B. Zineb, and S. Tabbane, "A UHF path loss model using learning machine for heterogeneous networks," *IEEE Trans. Antennas Propag.*, vol. 65, no. 7, pp. 3675–3683, Jul. 2017, doi: 10.1109/TAP.2017.2705112.

[14] M. Hatay, "Empirical formula for propagation loss in land mobile radio services," *IEEE Trans. Veh. Technol.*, vol. VT-29, no. 3, pp. 317–325, Aug. 1980, doi: 10.1109/T-VT.1980.23859.

[15] Y. D. J. Bultitude and T. Rautiainen. (2007). *IST-4-027756 WINNER II. D1.1.2 V1.2. WINNER II Channel Models*. EBITG, TUI, UOULU, CU/CRC, NOKIA. [Online]. Available: https://signserv.signal.uu.se/Publications/WINNER/WIN2D112.pdf

[16] ITU-R Series P. (2009). *P.1812 : A Path-Specific Propagation Prediction Method for Point-to-Area Terrestrial Services in the VHF and UHF Bands*. [Online]. Available: https://www.itu.int/dms_pubrec/itu-r/rec/p/R-REC-P.1812-4-201507-I!!PDF-E.pdf

[17] V. Erceg and K. Hari. (2000). *Channel Models for Broadband Fixed Wireless Systems*. IEEE 802.16. 3c-00. [Online]. Available: https://www.ieee802.org/16/tg3/contrib/802163c-01_29r4.pdf

[18] P. L. Rice, A. G. Longley, K. Norton, and A. Barsis. (1965). *Transmission Loss Predictions for Tropospheric Communication Circuits*. U.S. Department of Commerce, National Bureau of Standards. [Online]. Available: https://apps.dtic.mil/dtic/tr/fulltext/u2/687820.pdf

[19] K. Paran and N. Noori, "Tuning of the propagation model ITU-R P. 1546 recommendation," *Prog. Electromagn. Res.*, vol. 8, pp. 243–255, 2008. [Online]. Available: https://www.jpier.org/PIERB/pier.php?paper=08062201

[20] A. Neskovic, N. Neskovic, and D. Paunovic, "Indoor electric field level prediction model based on the artificial neural networks," *IEEE Commun. Lett.*, vol. 4, no. 6, pp. 190–192, Jun. 2000, doi: 10.1109/4234.848409.

[21] F. M. Landstorfer, "Empirical prediction of radiowave propagation by neural network simulator," *Electron. Lett.*, vol. 28, no. 8, pp. 724–726, Apr. 1992, doi: 10.1049/ip-h-2.1993.0048.

[22] Z. Stankovic, B. Milovanvic, M. Veljkovic, and A. Dordevic, "The hybrid-neural empirical model for the electromagnetic field level prediction in urban environments," in *Proc. 7th Seminar Neural Netw. Appl. Electr. Eng. (NEUREL)*, 2004, pp. 189–192. [Online]. Available: https://www.academia.edu/9716245/The_hybrid_neural_empirical_model_for_the_electromagnetic_field_level_prediction_in_urban_environments

[23] I. Popescu, D. Nikitopoulos, P. Constantinou, and I. Nafornita, "ANN prediction models for outdoor environment," in *Proc. IEEE 17th Int. Symp. Pers., Indoor Mobile Radio Commun.*, Sep. 2006, pp. 1–5, doi: 10.1109/PIMRC.2006.254270.

[24] H. K. Rath, S. Timmadasari, B. Panigrahi, and A. Simha, "Realistic indoor path loss modeling for regular WiFi operations in India," in *Proc. 23rd Nat. Conf. Commun. (NCC)*, Mar. 2017, pp. 1–6, doi: 10.1109/NCC.2017.8077107.

[25] N. O. Oyie and T. J. O. Afullo, "Measurements and analysis of large-scale path loss model at 14 and 22 GHz in indoor corridor," *IEEE Access*, vol. 6, pp. 17205–17214, 2018, doi: 10.1109/ACCESS.2018.2802038.

[26] S. Ju, Y. Xing, O. Kanhere, and T. S. Rappaport, "Millimeter wave and sub-terahertz spatial statistical channel model for an indoor office building," *IEEE J. Sel. Areas Commun.*, vol. 39, no. 9, pp. 1561–1575, Jun. 2021, doi: 10.1109/JSAC.2021.3071844.

[27] Y. Xing, T. S. Rappaport, and A. Ghosh, "Millimeter wave and sub-THz indoor radio propagation channel measurements, models, and comparisons in an office environment," 2021, *arXiv:2103.00385*.

[28] J. Ko, Y.-J. Cho, S. Hur, T. Kim, J. Park, A. F. Molisch, K. Haneda, M. Peter, D.-J. Park, and D.-H. Cho, "Millimeter-wave channel measurements and analysis for statistical spatial channel model in in-building and urban environments at 28 GHz," *IEEE Trans. Wireless Commun.*, vol. 16, no. 9, pp. 5853–5868, Jun. 2017, doi: 10.1109/TWC.2017.2716924.

[29] T. S. Rappaport, G. R. Maccartney, M. K. Samimi, and S. Sun, "Wideband millimeter-wave propagation measurements and channel models for future wireless communication system design," *IEEE Trans. Commun.*, vol. 63, no. 9, pp. 3029–3056, Sep. 2015, doi: 10.1109/TCOMM.2015.2434384.

[30] T. S. Rappaport, "Characterization of UHF multipath radio channels in factory buildings," *IEEE Trans. Antennas Propag.*, vol. 37, no. 8, pp. 1058–1069, Aug. 1989, doi: 10.1109/8.34144.

[31] P. Kyosti. (2007). *WINNER II Channel Models*. IST, IST-4-027756 WINNER II D1. 1.2 V1. 2. [Online]. Available: https://signserv.signal.uu.se/Publications/WINNER/WIN2D112.pdf

[32] G. R. MacCartney, J. Zhang, S. Nie, and T. S. Rappaport, "Path loss models for 5G millimeter wave propagation channels in urban microcells," in *Proc. IEEE Global Commun. Conf. (GLOBECOM)*, Dec. 2013, pp. 3948–3953, doi: 10.1109/GLOCOM.2013.6831690.

[33] M. K. Samimi, T. S. Rappaport, and G. R. MacCartney, Jr., "Probabilistic omnidirectional path loss models for millimeter-wave outdoor communications," *IEEE Wireless Commun. Lett.*, vol. 4, no. 4, pp. 357–360, Aug. 2015, doi: 10.1109/LWC.2015.2417559.

[34] A. I. Sulyman, A. T. Nassar, M. K. Samimi, G. R. MacCartney, Jr., T. S. Rappaport, and A. Alsanie, "Radio propagation path loss models for 5G cellular networks in the 28 GHz and 38 GHz millimeter-wave bands," *IEEE Commun. Mag.*, vol. 52, no. 9, pp. 78–86, Sep. 2014, doi: 10.1109/MCOM.2014.6894456.

[35] C. O. Mgbe, J. M. Mom, and G. A. Igwue, "Performance evaluation of generalized regression neural network path loss prediction model in macrocellular environment," *Perform. Eval.*, vol. 2, no. 2, pp. 1–5, 2015. [Online]. Available: https://www.jmest.org/wp-content/uploads/JMESTN42350486.pdf

[36] M. Piacentini and F. Rinaldi, "Path loss prediction in urban environment using learning machines and dimensionality reduction techniques," *Comput. Manage. Sci.*, vol. 8, no. 4, pp. 371–385, 2011, doi: 10.1007/s10287-010-0121-8.

[37] V. Kecman, *Learning and Soft Computing: Support Vector Machines, Neural Networks, and Fuzzy Logic Models*. Cambridge, MA, USA: MIT Press, 2001. [Online]. Available: https://www.amazon.com/Learning-Soft-Computing-Machines-Networks/dp/0262527901

[38] H. Musafer, A. Abuzneid, M. Faezipour, and A. Mahmood, "An enhanced design of sparse autoencoder for latent features extraction based on trigonometric simplexes for network intrusion detection systems," *Electronics*, vol. 9, no. 2, p. 259, 2020. [Online]. Available: https://www.mdpi.com/2079-9292/9/2/259

[39] J. Wang, C. Jiang, H. Zhang, Y. Ren, K.-C. Chen, and L. Hanzo, "Thirty years of machine learning: The road to Pareto-optimal wireless networks," *IEEE Commun. Surveys Tuts.*, vol. 22, no. 3, pp. 1472–1514, 3rd Quart., 2020, doi: 10.1109/COMST.2020.2965856.

[40] T. S. Rappaport, "Wireless communications–principles and practice, (the book end)," *Microw. J.*, vol. 45, no. 12, pp. 128–129, 2002.

[41] S. Sun, T. S. Rappaport, R. W. Heath, Jr., A. Nix, and S. Rangan, "MIMO for millimeter-wave wireless communications: Beamforming, spatial multiplexing, or both?" *IEEE Commun. Mag.*, vol. 52, no. 12, pp. 110–121, Dec. 2014, doi: 10.1109/MCOM.2014.6979962.

[42] *Technical Specification Group Radio Access Network; Study on Scenarios and Requirements for Next Generation Access Technologies;(Release 14)*, document G. T. 38.913, 2016.

[43] M. K. Samimi and T. S. Rappaport, "3-D millimeter-wave statistical channel model for 5G wireless system design," *IEEE Trans. Microw. Theory Techn.*, vol. 64, no. 7, pp. 2207–2225, Jul. 2016, doi: 10.1109/TMTT.2016.2574851.

[44] A. Hrovat, G. Kandus, and T. Javornik, "Path loss analyses in tunnels and underground corridors," *Int. J. Commun.*, vol. 6, no. 3, pp. 136–144, Aug. 2012. [Online]. Available: https://naun.org/main/NAUN/communications/17-875.pdf

[45] A. Emslie, R. Lagace, and P. Strong, "Theory of the propagation of UHF radio waves in coal mine tunnels," *IEEE Trans. Antennas Propag.*, vol. AP-23, no. 2, pp. 192–205, Mar. 1975, doi: 10.1109/TAP.1975.1141041.

[46] Y. P. Zhang, Y. Hwang, and J. D. Parsons, "UHF radio propagation characteristics in straight open-groove structures," *IEEE Trans. Veh. Technol.*, vol. 48, no. 1, pp. 249–254, Jan. 1999, doi: 10.1109/25.740100.

FEYISA DEBO DIBA received the B.Sc. degree in electrical engineering from Arba Minch University, Arba Minch, Ethiopia, in 2006, the M.Sc. degree in communication engineering from Addis Ababa University, Addis Ababa, Ethiopia, in 2010, and the Ph.D. degree in electronic/telecommunication engineering from the University of KwaZulu-Natal, Durban, South Africa, in 2017.

He did a Postdoctoral Fellowship in mm wave propagation channel measurements and modeling for 5G and beyond at Chosun University, Gwangju, South Korea, from 2020 to 2021. He is currently a Postdoctoral Researcher at Ulsan University, South Korea. His current research interests include wireless communication networking and optimization, energy networking and optimization, and mm wave propagation for 5G and beyond. He was a recipient of the South African Institute of Electrical Engineers Annual Award for journal article published in September 2016 issue of *SAIEE Africa Research Journal*.

MD ABDUS SAMAD (Member, IEEE) is currently pursuing the Ph.D. degree in information and communication engineering with Chosun University, Gwangju, South Korea.

Since 2013, he has been an Assistant Professor with the Department of Electronics and Telecommunication Engineering, International Islamic University Chittagong, Chattogram, Bangladesh. His research interests include signal processing, antenna design, electromagnetic wave propagation, applications of artificial neural networks, and deep learning and attenuation of millimeter-wave propagation by interference or atmospheric causes for 5G and beyond wireless networks. He won the prestigious Korean Government Scholarship (GKS) for his Ph.D. degree, in 2017.

DONG-YOU CHOI (Senior Member, IEEE) received the B.S., M.S., and Ph.D. degrees from the Department of Electronic Engineering, Chosun University, Gwangju, South Korea, in 1999, 2001, and 2004, respectively. Since 2006, he has been a Professor with the Department of Information and Communication Engineering, Chosun University. His research interests include rain attenuation, antenna design, wave propagation, and microwave and satellite communication. He is a member of the KEES, IEEK, and KICS.

● ● ●